Supporting Information

Extraction of Photogenerated Electrons and Holes from a COF Integrated Heterojunction

Mona Calik,‡ Florian Auras,‡ Laura M. Salonen,‡ Kathrin Bader, Irene Grill, Matthias Handloser, Dana D. Medina, Mirjam Dogru, Florian Löbermann, Dirk Trauner, Achim Hartschuh, Thomas Bein*

Department of Chemistry and Center for NanoScience (CeNS), University of Munich (LMU), Butenandtstrasse 5-13, 81377 Munich, Germany

Table of contents

Abbreviations

BET = Brunauer–Emmett–Teller; CC = column chromatography; DDQ = 2,3-dichloro-5,6-dicyano-1,4-benzoquinone; EtOAc = ethyl acetate; FWHM = full width at half maximum; HHTP = 2,3,6,7,10,11-hexahydroxytriphenylene; Mp = melting point; QSDFT = quenched solid density functional theory; R_f = retardation factor; RT = room temperature; THF = tetrahydrofuran.

Section 1: Materials and methods

Unless stated otherwise, all reactions were performed in oven-dried glassware under a positive pressure of Ar. Commercial reagents and solvents were used as received with the exception of pyrrole, which was distilled prior to use using a rotary evaporator. Reactions were stirred magnetically and monitored by NMR spectroscopy or analytical thin-layer chromatography (TLC) using E. Merck 0.25 mm silica gel 60 F254 pre-coated glass plates. TLC plates were visualized by exposure to ultraviolet light (254 nm). Flash column chromatography was performed employing silica gel (60 Å, 40–63 μm, Merck).

Nuclear magnetic resonance (NMR) spectra were recorded on Varian VNMRS 300, VNMRS 400, INOVA 400 or VNMRS 600 spectrometers. Proton chemical shifts are expressed in parts per million (δ scale) and are calibrated using residual undeuterated solvent peak as an internal reference ($CDCl_3$: δ 7.26; THF-d_8: δ 1.72, 3.58). Data for ^{1}H NMR spectra are reported as follows: chemical shift (δ ppm) (multiplicity, coupling constant/Hz, integration). Multiplicities are reported as follows: s = singlet, d = doublet, t = triplet, q = quartet, m = multiplet, br = broad, or combinations thereof. Carbon chemical shifts are expressed in ppm (δ scale) and are referenced to the carbon resonances of the solvent ($CDCl_3$: δ 77.16; THF-d_8: δ 67.21, 25.31).

Infrared (IR) spectra were recorded on a Perkin Elmer Spectrum BX II FT-IR system and a Thermo Scientific Nicolet™ 6700 FT-IR spectrometer in transmission mode. IR data is reported in frequency of absorption (cm^{-1}).

Mass spectrometry (MS) experiments were performed on a Thermo Finnigan MAT 95 (EI) or on a Thermo Finnigan LTQ FT (ESI) instrument.

The nitrogen sorption isotherm was recorded on a Quantachrome Autosorb 1 at 77.35 K in a pressure range from p/p^0 = 0.001 to 0.98. Prior to the measurement of the sorption isotherm the sample was heated for 24 h at 120°C under turbomolecular pump vacuum. For the evaluation of the surface area the BET model was applied between 0.05 and 0.2 p/p^0. The calculation of the pore size distribution was done using the QSDFT equilibrium model with a carbon kernel for cylindrical pores.

The permanent porosity of COF films was assessed by a krypton sorption measurement of degassed films (24 h at RT *in vacuo*). The isotherm was recorded at 77 K on a Quantachrome autosorb iQ instrument in a pressure range from p/p^0 = 0.002 to 0.95 using a vacuum volumetric technique.

X-ray diffraction (XRD) measurements were performed using a Bruker D8 Discover with Ni-filtered Cu K_α radiation and a LynxEye position-sensitive detector.

Transmission electron microscopy was performed on an FEI Titan 80-300 equipped with a field emission gun operated at 80 kV. Scanning electron microscopy (SEM) images were recorded with a JEOL 6500F field emission microscope operated at 5 kV using a secondary electron detector.

UV-Vis spectra were recorded using a Perkin-Elmer Lambda 1050 spectrometer equipped with a 150 mm integrating sphere. Absorbance spectra of COF thin films were corrected for the transmission of the substrate and reflection losses.

Photoluminescence (PL) measurements were performed using a home-built setup consisting of a Horiba Jobin Yvon iHR 320 monochromator equipped with a photomultiplier tube and a liquid N_2-

cooled InGaAs detector. The samples were illuminated with a pulsed (83 Hz) 405 nm LED at a light intensity of 500 mW cm^{-2}.

Differential pulse voltammetry (DPV) was measured using 50 μM solutions of **1** and HHTP in acetonitrile or a 3:5 mixture of acetonitrile/1,4-dioxane, respectively, with 0.1 M tetrabutylammonium hexafluorophosphate as electrolyte and 0.1 mM ferrocene as internal reference. Measurements were performed with a Metrohm Autolab PGSTAT302N potentiostat, using Pt wires as the working electrode and counter electrode and a saturated Ag/AgCl reference electrode (Sigma Aldrich, 0.197 V vs. SHE).

Photovoltaic devices were tested under illumination from an AM1.5G solar simulator (Solar Light Model 16S), which was calibrated to 100 mW cm^{-2} using a Fraunhofer ISE certified KG5 filtered silicon cell. Current-voltage (*J*-*V*) curves were recorded with a Keithley 2400 source-measure unit.

External quantum efficiency (EQE) measurements were performed at short circuit unless stated otherwise, and referenced to a Si photodiode with NIST traceable calibration. The device under test was illuminated with chopped (f = 7 Hz) monochromatic light. The current response was detected via a lock-in amplifier (Signal Recovery SR7230) with a low-noise pre-amplifier.

Photoinduced absorption measurements were carried out in transmission geometry using a stabilized continuum white light source in combination with a chopped excitation laser (f_{chop} = 1 kHz, λ_{exc} = 470 nm). Photoinduced changes in transmission through the thin film were recorded by a photodiode via lock-in detection (SRS 830). Photoinduced absorption spectra in the transparency range of the film were recorded by selecting different detection wavelengths using narrow bandpass filters each having a FWHM of 10 nm.

Section 2: Synthesis

The synthesis of boronic acid porphyrin **1** started with preparation of dipyrromethane **2**[1] from pyrrole (**3**) and paraformaldehyde (**4**) (Scheme S1). Then, in a procedure adapted from the literature,[2] boronic ester-bearing aldehyde **5**, previously obtained by protection of boronic acid **6**, was reacted with dipyrromethane to yield porphyrin **7** in 30% yield. Finally, acidic deprotection of the boronic ester moieties gave access to porphyrin **1** in 77% yield.

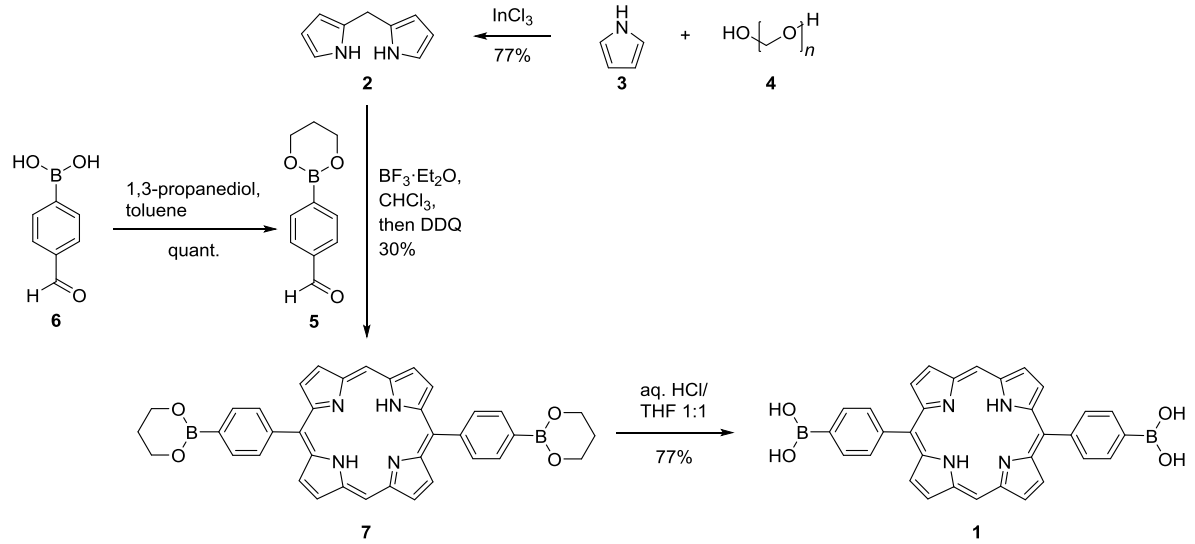

Scheme S1. Synthesis of boronic acid porphyrin **1**.

5,15-Bis(4-boronophenyl)porphyrin (1)

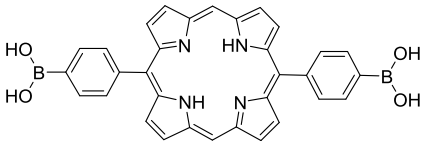

Porphyrin **7** (1.08 g, 1.71 mmol, 1 equiv.) was stirred in a mixture of THF (450 mL) and aq. HCl solution (450 mL, pH = 1) in the dark at RT for 24 h. Then, CH_2Cl_2 (650 mL) was added, and the precipitated product collected by filtration. The solid was suspended in MeOH, centrifuged, and MeOH was decanted off. The procedure was repeated three times to give **1** (640 mg, 77%) as purple solid.

Mp > 305 °C (decomp); ^{1}H NMR (400 MHz, THF-d_8+3 drops of D_2O): 8.20 (d, J = 8.1 Hz, 4H), 8.30 (d, J = 8.1 Hz, 4H), 9.03 (d, J = 4.6 Hz, 4H), 9.47 (d, J = 4.6 Hz), 10.42 (s, 2H); ^{13}C NMR (100 MHz, THF-d_8): 106.2, 111.1, 120.1, 131.5, 132.7, 133.9, 134.9, 143.9 (2 signals invisible); IR (ATR): 3282, 1604, 1577, 1471, 1395, 1321, 1236, 1197, 1145, 1103, 1008, 973, 954, 850, 786, 745, 732, 718, 688; HR-ESI-MS: m/z: 551.2048 ([M+H]$^+$, calculated for $C_{32}H_{25}B_2N_4O_4^+$: 551.2057).

Di(1*H*-pyrrol-2-yl)methane[1] **(2)**

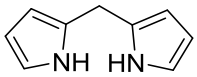

A suspension of paraformaldehyde (**4**) (1.63 g, 54.4 mmol, 1 equiv.) in pyrrole (**3**) (350 mL, 5040 mmol, 93 equiv.) was degassed with Ar for 15 min. The mixture was heated to 55 °C for 10 min before the addition of $InCl_3$ (1.19 g, 5.38 mmol, 0.1 equiv.). The mixture was stirred at 55 °C for 3 h, cooled down, and treated with powdered NaOH (7.20 g, 180 mmol, 3.3 equiv.). After 1 h at RT, the mixture was filtered over celite, washed with pyrrole, and evaporated to dryness. Purification by CC (SiO_2; packed with isohexane, elution isohexane/EtOAc 9:1) gave **2** (6.15 g, 77%) as off-white solid.

R_f = 0.57 (isohexane/EtOAc 2:1); ^{1}H NMR (600 MHz, $CDCl_3$): 3.97 (s, 2H), 6.05 (dddt, J = 3.3, 2.5, 1.6, 0.8 Hz, 2H), 6.16 (q, J = 2.9 Hz, 2H), 6.64 (td, J = 2.6, 1.6 Hz, 2H), 7.78 (br s, 2H); ^{13}C NMR (150 MHz, $CDCl_3$): 26.5, 106.5, 108.5, 117.4, 129.2; HR-EI-MS: m/z (%): 146.0837 (100, [M]$^+$, calculated for $C_9H_{10}N_2^+$: 146.0844).

4-(1,3,2-Dioxaborinan-2-yl)benzaldehyde[3] **(5)**

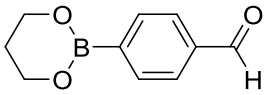

In a flask equipped with a Dean-Stark trap, a suspension of 4-formylphenylboronic acid (**6**) (10.2 g, 68.0 mmol, 1 equiv.) and 1,3-propanediol (5.20 mL, 72.4 mmol, 1.1 equiv.) in toluene (510 mL) was heated at 135 °C for 5 h. The mixture was evaporated to dryness to give **5** (13 g, quant.) as white solid.

Mp = 60–62 °C; ^{1}H NMR (300 MHz, $CDCl_3$): 2.05–2.12 (m, 2H), 4.19 (t, *J* = 5.5 Hz, 4H), 7.84 (d, *J* = 8.3 Hz, 2H), 7.92 (d, *J* = 8.1 Hz, 2H), 10.04 (s, 1H); ^{13}C NMR (75 MHz, $CDCl_3$): 27.5, 62.3, 128.8, 134.3, 137.9, 193.0 (1 signal invisible); IR (ATR): 2976, 2949, 2897, 2823, 2731, 1695, 1658, 1564, 1505, 1486, 1477, 1429, 1386, 1340, 1308, 1296, 1268, 1207, 1175, 1153, 1126, 1104, 1001, 921, 852, 826, 727, 672; HR-EI-MS: *m*/*z* (%): 189.0717 (100, [*M*–H]$^+$, calculated for $C_{10}H_{10}BO_3^+$: 189.0723).

5,15-Bis(4-(1,3,2-dioxaborinan-2-yl)-phenyl)porphyrin (7)

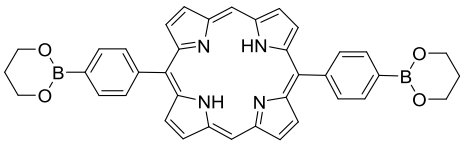

Compounds **2** (1.66 g, 11.4 mmol, 1 equiv.) and **5** (2.14 g, 11.2 mmol, 1 equiv.) were dissolved in anhydrous $CHCl_3$ (1 L) under Ar, and the mixture was degassed with Ar for 15 min. The reaction mixture was cooled to 0 °C, BF_3•OEt_2 (320 µL, 2.53 mmol, 0.2 equiv.) was added, and the mixture was stirred for 3 h at RT. Then, DDQ (4.16 g, 18.3 mmol, 1.6 equiv.) was added in one portion, and the mixture was stirred overnight at RT. The mixture was filtered over celite, and poured on to a column of silica (CH_2Cl_2; elution CH_2Cl_2/MeOH 100:1). The collected purple solid was recrystallized from $CHCl_3$ to give **7** (1.08 g, 30%) as dark purple solid.

R_f = 0.44 (CH_2Cl_2/MeOH 95:5); Mp = 370 °C (decomp); ^{1}H NMR (600 MHz, $CDCl_3$): –3.10 (s, 2H), 2.25 (quintet, *J* = 5.5 Hz, 4H), 4.37 (t, *J* = 5.6 Hz, 8H), 8.21–8.28 (m, 8H), 9.07 (d, *J* = 4.5 Hz, 4H), 9.39 (d, *J* = 4.5 Hz, 4H), 10.31 (s, 2H); ^{13}C NMR (150 MHz, $CDCl_3$): 27.8, 62.4, 105.4, 119.4, 131.2, 131.7, 132.4, 134.5, 143.7, 145.3, 147.2 (1 signal invisible); IR (ATR): 2935, 2884, 1603, 1579, 1546, 1478, 1417, 1389, 1334, 1302, 1272, 1209, 1150, 1123, 1053, 1005, 992, 986, 972, 955, 864, 855, 795, 751, 735, 718, 693, 664; HR-EI-MS: *m*/*z* (%): 630.2613 (100, [*M*]$^+$, calculated for $C_{38}H_{32}B_2N_4O_4^+$: 630.2610).

TP-Por COF

For the synthesis of TP-Por COF 11.5 mg of compound **1** (0.02 mmol, 3 equiv.) and 4.5 mg of HHTP (0.014 mmol, 2 equiv.) were added to a Teflon-lined steel autoclave and dispersed in a solvent mixture of acetonitrile and mesitylene (7:3 *v*:*v*, 1 mL). The autoclave was placed in an oven at 120 °C for 72 h. After the time had elapsed, the reaction mixture was allowed to cool down to room temperature and the resulting powder was then collected by filtration through a Hirsch funnel. After washing the product three times with dry toluene it was left under dynamic vacuum to come to complete dryness.

TP-Por COF films

11.5 mg of compound **1** (0.02 mmol, 3 equiv.) and 4.5 mg HHTP (0.014 mmol, 2 eq) were added to a 100 mL Schott flask and dissolved in a solvent mixture of acetonitrile and mesitylene in a 7:3 *v*:*v* ratio (30 mL). The substrates (fused silica or ITO-covered glass), covered with a 10 nm layer of vacuum-deposited MoO_x, were placed face down in the reaction solution. The flask was heated in an oven at 120 °C for 18 h. After the reaction mixture had cooled down to room temperature, the films were removed from the flask and washed by a short sonication treatment (2 s) in toluene. The obtained films were dried under a nitrogen flow prior to characterization.

Device fabrication

A stock solution of 5–6 nm ZnO nanocrystals in *n*-BuOH/MeOH/$CHCl_3$ 88:6:6 *v*:*v*:*v* was prepared following literature procedures.[4] This solution was sonicated for 15 min prior to use.

The COF-based device was prepared on ITO-coated glass (VisonTec, 12–15 ohms/sq) slides. A 10 nm thick MoO_x electron blocking layer was deposited by thermal evaporation. A COF thin film was subsequently grown on this substrate as described above. An electron-selective contact was applied by spin-coating a dispersion of ZnO nanocrystals, resulting in a layer thickness of about 20 nm. The device was completed by thermal evaporation of 80 nm thick Al contacts in high vacuum through a shadow mask, thus defining an active area of 3×3 mm^2 for each device.

For the reference device based on a blend of the building blocks, 1.65 mg (3.0 μmol) of compound **1** and 0.65 mg (2.0 μmol) HHTP were dissolved in 200 μL 1,3-dioxolane and 100 μL MeOH. This solution was spin-cast onto a MoO_x-coated ITO substrate, yielding an active layer of ~40 nm thickness. Subsequently, a 10 nm layer of poly[(9,9-bis(2,2'-*N*,*N*'-dimethylaminopropyl)fluorenyl-2,7-diyl)-*alt*-*co*-(9,9-dioctylfluorenyl-2,7-diyl)] (PFN; Solaris Chem), serving as an electron-selective contact, was spin-coated from a 2 mg mL^{-1} methanol solution containing 5 μL glacial acetic acid. The device was completed by thermal evaporation of 120 nm Al contacts.

Section 3: Simulation of the TP-Por COF crystal structure

To determine the crystal structure of the obtained product, a powder diffraction pattern was calculated based on a simulated crystal structure. The unit cell was constructed using the Materials Studio software and optimized by force field calculations. Due to the non-planar porphyrin building block, the unit cell is limited to a trigonal *P3* symmetry in the case of an eclipsed stacked structure and $P6_3$ symmetry for a staggered arrangement. The comparison of the calculated pattern with the experimental data identified the obtained structure as AA stacked TP-Por COF.

Table S1. Refined crystal data.

Formula	$C_{132}\ H_{72}\ B_6\ N_{12}\ O_{12}$
Formula weight	2082.96 g mol^{-1}
Crystal system	trigonal
Space-group	*P3*
Cell parameters	$a = b = 52.2$ Å, $c = 3.8$ Å
Cell volume	8977 $Å^3$

Table S2. Fractional atomic coordinates.

Atom	Wyck.	x	y	z
C1	3d	0.91955	0.94724	-0.01394
N2	3d	0.69905	0.87622	-0.01391
C3	3d	0.72863	0.88841	0.02061
C4	3d	0.742	0.91883	0.06597
C5	3d	0.71977	0.92569	0.05331
C6	3d	0.82388	0.9315	-0.21349
C7	3d	0.793	0.91588	-0.21168
C8	3d	0.9457	1.00046	-0.03098
C9	3d	0.97289	1.00079	-0.02418
C10	3d	0.4139	0.72073	0.03347
N11	3d	0.63444	0.79159	0.03275
C12	3d	0.63945	0.76894	0.08877
C13	3d	0.60489	0.77964	0.06862
C14	3d	0.59155	0.74965	0.15129
C15	3d	0.61379	0.74277	0.16147
C16	3d	0.50943	0.73532	-0.15931
C17	3d	0.54032	0.75089	-0.16343
O18	3d	0.44211	0.74513	0.04853
C19	3d	0.38758	0.66751	0.00825
C20	3d	0.36041	0.66725	0.02005

Atom	Wyck.	x	y	z
C28	3d	0.38765	0.72147	0.03575
C29	3d	0.36045	0.6946	0.02411
C30	3d	0.91949	0.97347	-0.03042
N31	3d	0.69904	0.82386	0.02666
C32	3d	0.69399	0.79595	0.0092
C33	3d	0.72858	0.84119	-0.01499
C34	3d	0.74185	0.82408	-0.06292
C35	3d	0.71962	0.795	-0.04449
C36	3d	0.82426	0.89354	0.189
C37	3d	0.79337	0.87827	0.19712
O38	3d	0.89131	0.96966	-0.04227
C39	3d	0.94583	0.94658	-0.01434
C40	3d	0.66674	0.89724	-0.03767
C41	3d	0.66672	0.77056	0.05815
C42	3d	0.83951	0.92024	-0.01474
B43	3d	0.87376	0.9374	-0.01955
C44	3d	0.5895	0.79531	0.01666
C45	3d	0.49401	0.74759	0.02058
C46	3d	0.55629	0.77871	0.01841
B47	3d	0.45971	0.73047	0.02151

C21	3d	0.41387	0.69447	0.01038
C22	3d	0.63943	0.87159	-0.06308
C23	3d	0.60486	0.82636	-0.03735
C24	3d	0.59148	0.843	-0.11765
C25	3d	0.61372	0.8721	-0.13138
C26	3d	0.50951	0.77532	0.19948
C27	3d	0.54041	0.79061	0.20144

C48	3d	0.69406	0.89911	0
O49	3d	0.89142	0.9228	0
N50	3d	0.63444	0.84395	0
O51	3d	0.44205	0.69821	0
C52	3d	0.744	0.87249	0
C53	3d	0.77723	0.8891	0
C54	3d	0.97284	0.97363	-0.02418

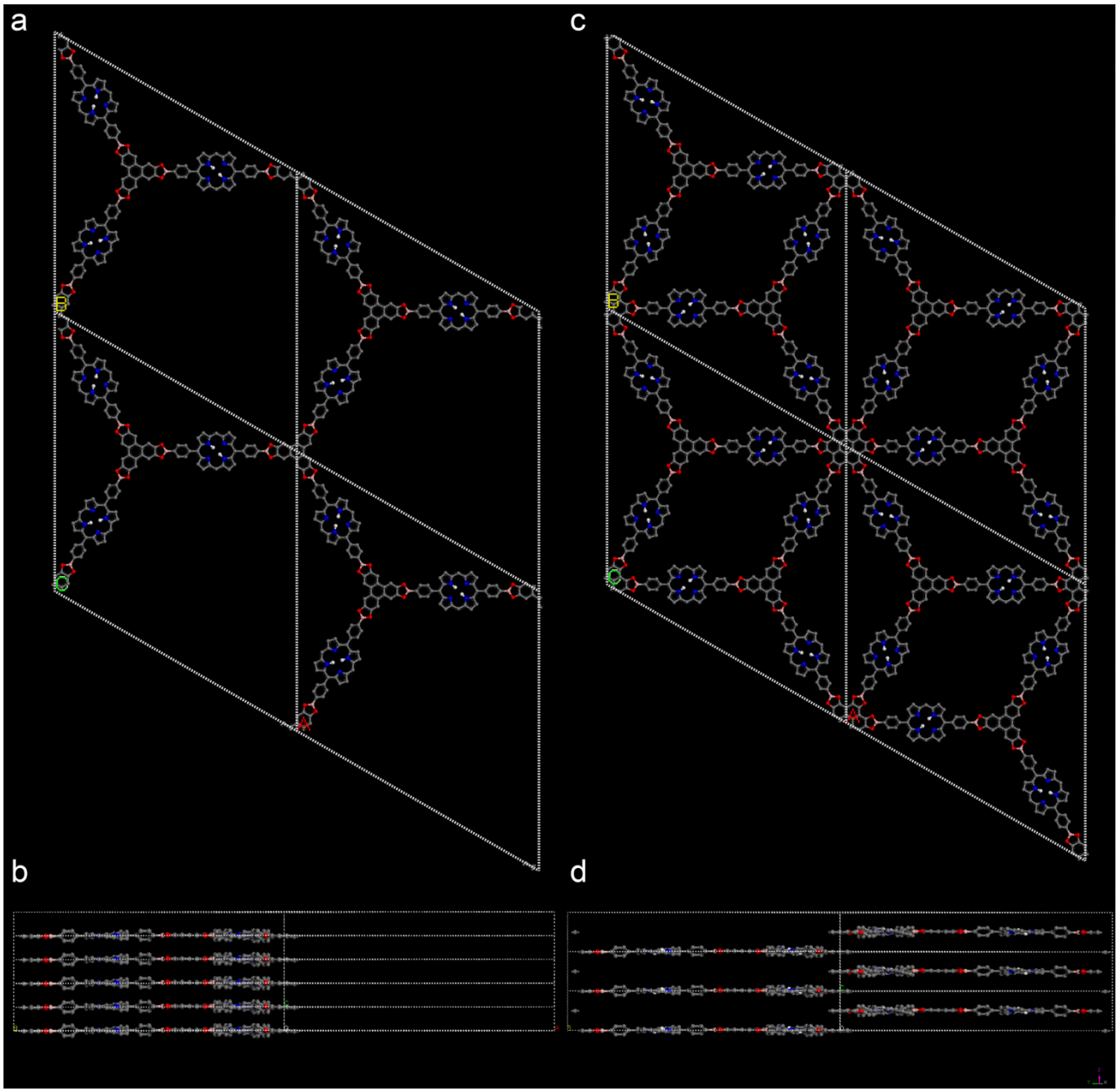

Figure S1. Simulation of the crystal lattice of TP-Por COF. a) Top view on the AB plane of 4 unit cells in an eclipsed stacking arrangement with *P3* symmetry, b) view along the *c*-axis of this fragment with an interlayer distance of 3.8 Å, c) view on the AB plane of 4 calculated unit cells of the TP-Por COF in a (hypothetical) staggered arrangement with $P6_3$ symmetry, and d) view along the c-axis with an interlayer distance of 6.5 Å.

Section 4: X-ray diffraction analysis of TP-Por COF thin films

To confirm the successful formation of TP-Por COF films on the conductive substrates they were analyzed by XRD in a detector scan mode. The XRD pattern shows a broad reflection at 24° 2θ, indicating oriented film growth with an interlayer distance of 3.8 Å (Figure S2).

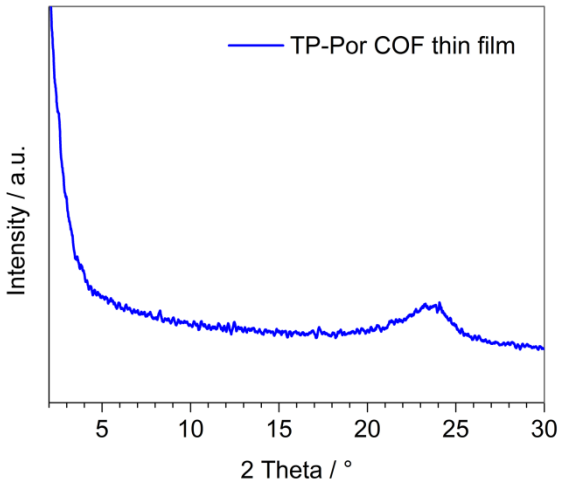

Figure S2. X-ray diffraction pattern of a TP-Por COF film measured in detector scan mode.

Section 5: Krypton sorption on COF thin films

The accessibility of the open pore system of TP-Por COF films was confirmed by krypton sorption measurements. The obtained type IV isotherm, which is characteristic for mesoporous materials, exhibits a sharp jump from 0.33 to 0.47 P/P_0, indicating a narrow pore size distribution.

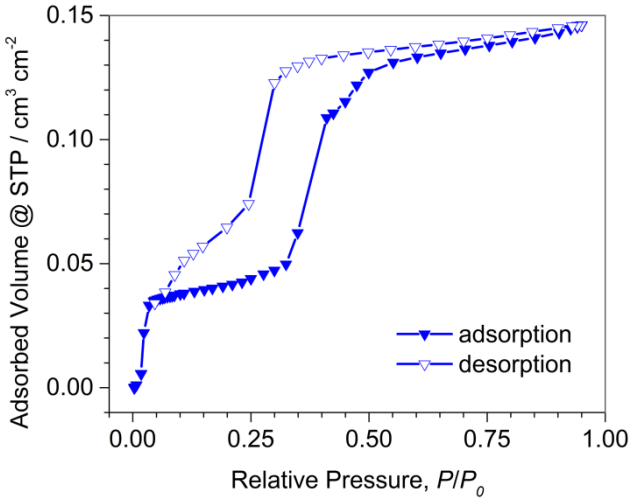

Figure S3. Krypton sorption isotherm of a TP-Por COF thin film measured at 77 K.

Section 6: IR spectroscopy

The successful formation of the boronate ester ring between HHTP and **1** was indicated by Fourier transform infrared (FTIR) spectroscopy through the appearance of the characteristic B–C stretching modes at 1333 cm^{-1} and 1261 cm^{-1} (Figure S4).[5]

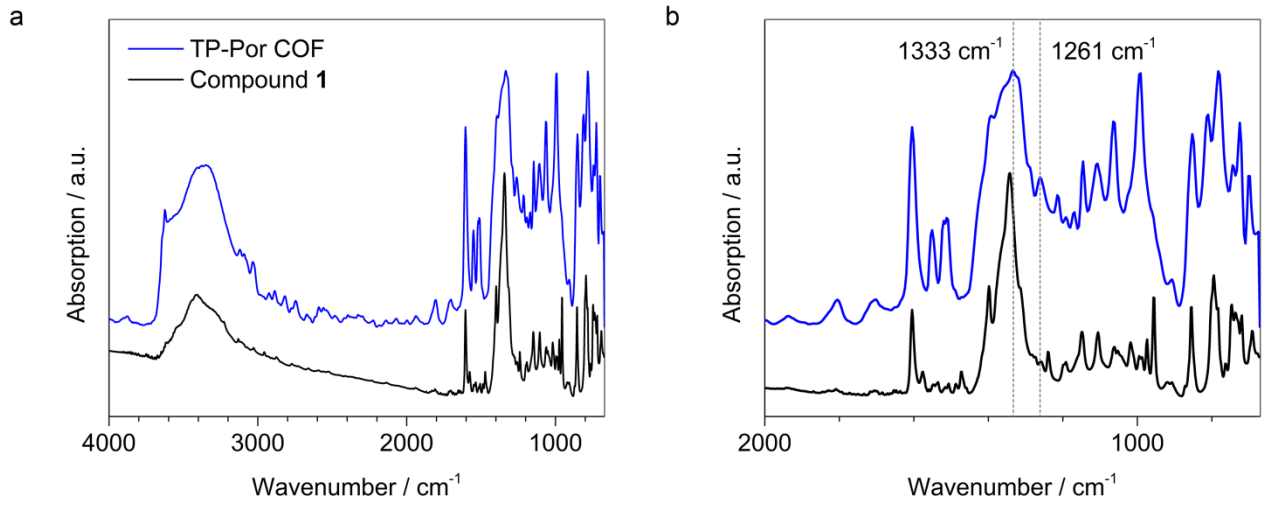

Figure S4. IR spectra of a TP-Por COF powder sample and the porphyrin diboronic acid **1**. a) Full range spectrum and b) enlargement of the region below 2000 cm^{-1} showing the characteristic signals of the B–C stretching modes at 1333 and 1261 cm^{-1}. The spectra were offset for clarity.

Table S3. Assignment of the most important IR-bands of TP-Por COF and Compound **1**.

Wavenumber / cm^{-1}	Assignment
1343	asymmetric B–O stretching mode (-$B(OH)_2$)
1333	"breathing" motion within the C_2O_2B ring
1315	symmetric B–C stretching mode(-$B(OH)_2$)
1261	coupled B–C and C=C stretching mode
1213	symmetric C–O stretching mode
1062	symmetric B–O stretching mode
972	coupled B–O stretch and O–H in plane bend(-$B(OH)_2$)
918	symmetric, in plane O–H bending (-$B(OH)_2$)

Section 7: UV-Vis spectroscopy

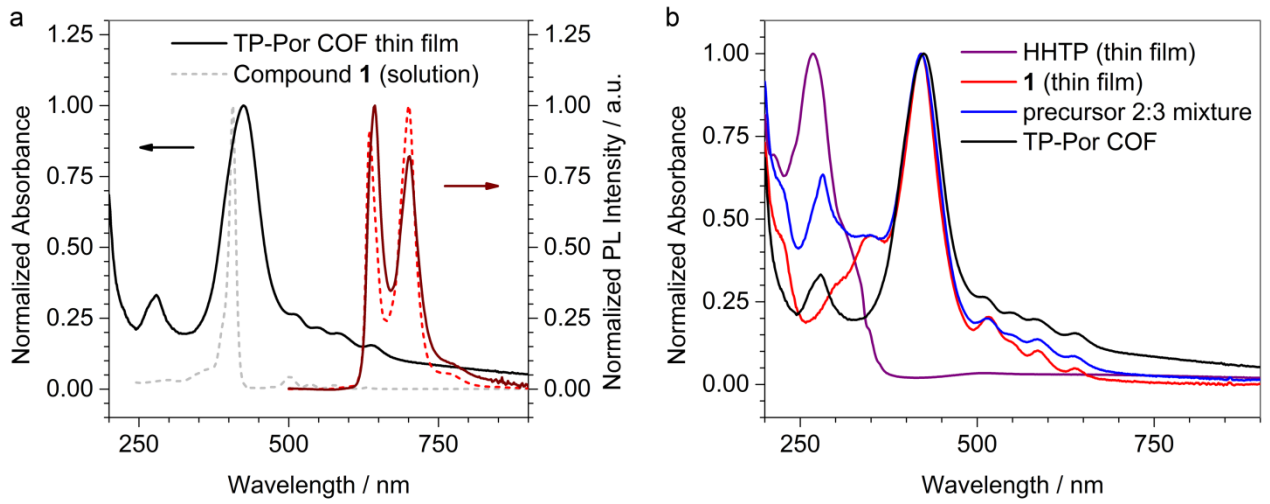

Figure S5. a) Absorption (black, grey) and photoluminescence emission spectra (brown, red) of a TP-Por COF thin film (solid line) and a 5 µM dioxane solution of the porphyrin diboronic acid **1** (dashed line). b) Comparison of the UV-Vis spectra of the TP-Por COF film (black) with spin-coated thin films of its precursors (purple and red for HHTP and **1**, respectively) and a 2:3 mixture of these precursors (blue).

Section 8: Differential pulse voltammetry and optical band gap of the COF building blocks

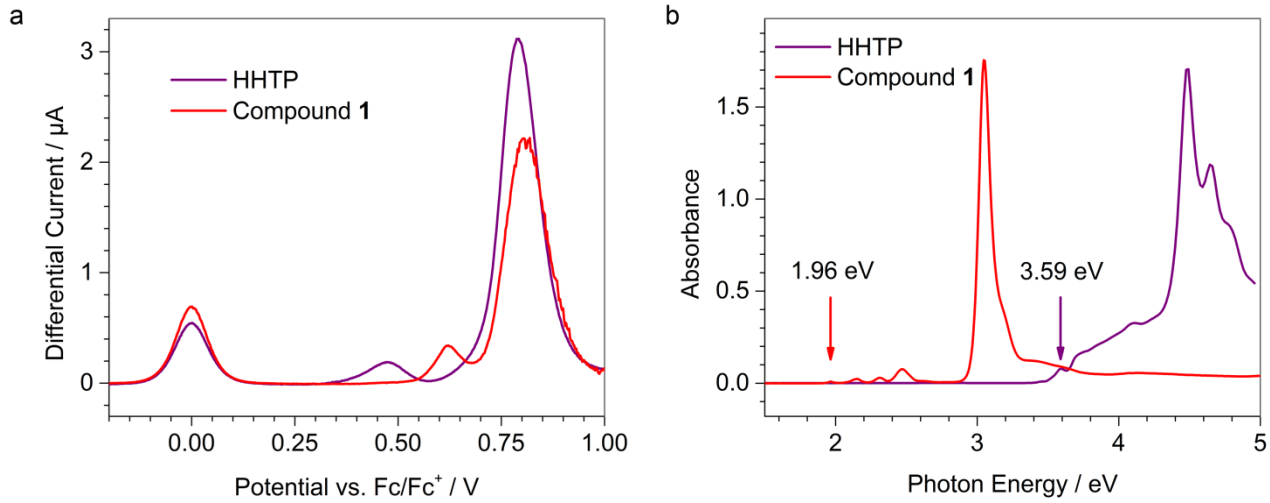

Figure S6. a) Differential pulse voltammograms of HHTP (purple) and **1** (red), measured towards more positive potentials (oxidation) and referenced to ferrocene. b) Corresponding UV-Vis spectra of the precursor solutions. The optical band gap is determined from the maximum of the lowest-energy optical transition.

Section 9: Additional optoelectronic characterization of the photovoltaic devices

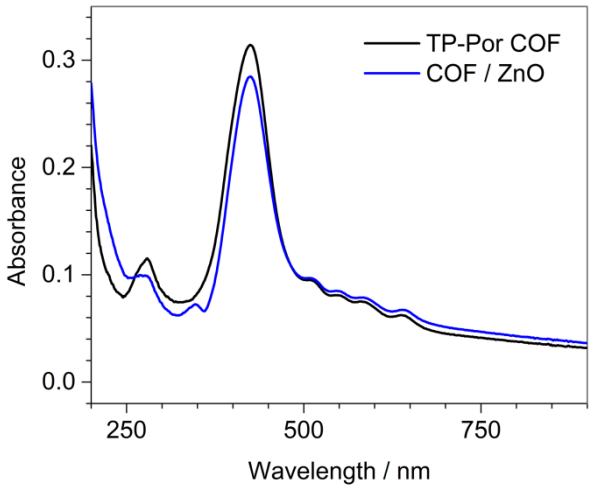

Figure S7. Transmission absorption spectra of a TP-Por COF thin film before (black) and after addition of the ZnO electron-selective layer. The additional feature at 347 nm can be ascribed to the ZnO nanocrystals.

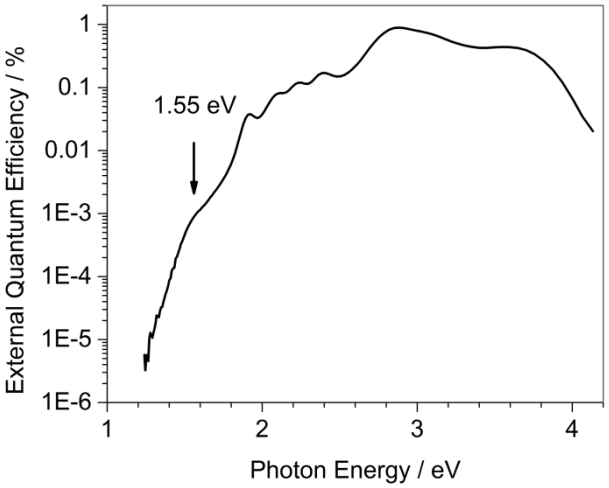

Figure S8. External quantum efficiency spectrum of a TP-Por COF-based photovoltaic device in semi-logarithmic representation. The defined feature at 1.55 eV might indicate the formation of a well-defined charge-transfer state inside the donor–acceptor framework.

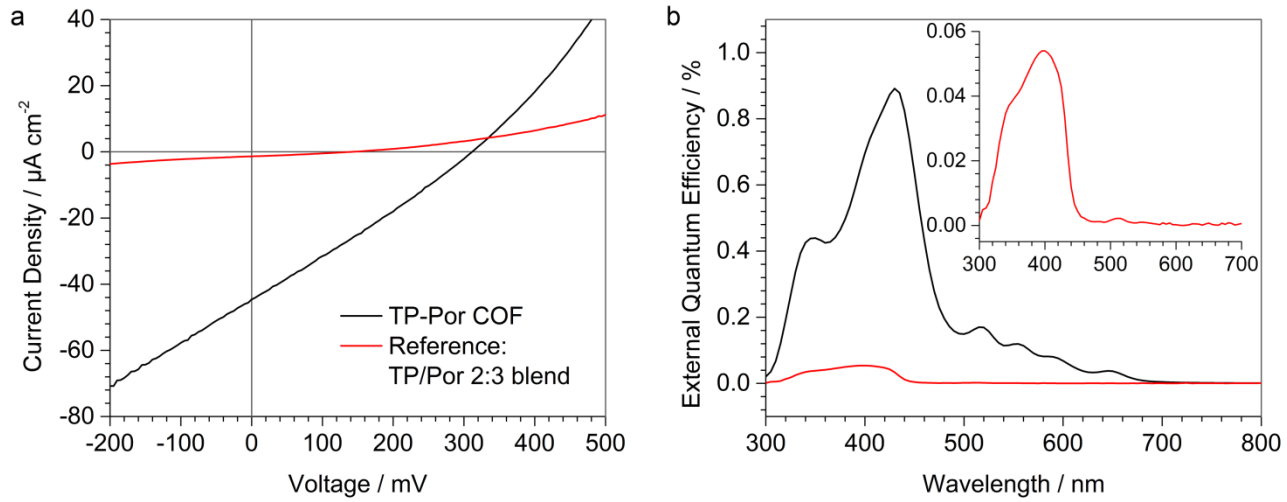

Figure S9. Comparison of a) the *J-V* curves recorded at 100 mW cm^{-2} AM1.5G illumination and b) EQE spectra of the TP-Por COF device (black) and the reference device based on a blend of the COF building blocks (red). The inset shows a magnified representation of the EQE spectrum of the TP/Por blend device.

Section 10: NMR spectroscopy

Compound **1**

400 MHz, THF-d_8+3 drops of D_2O

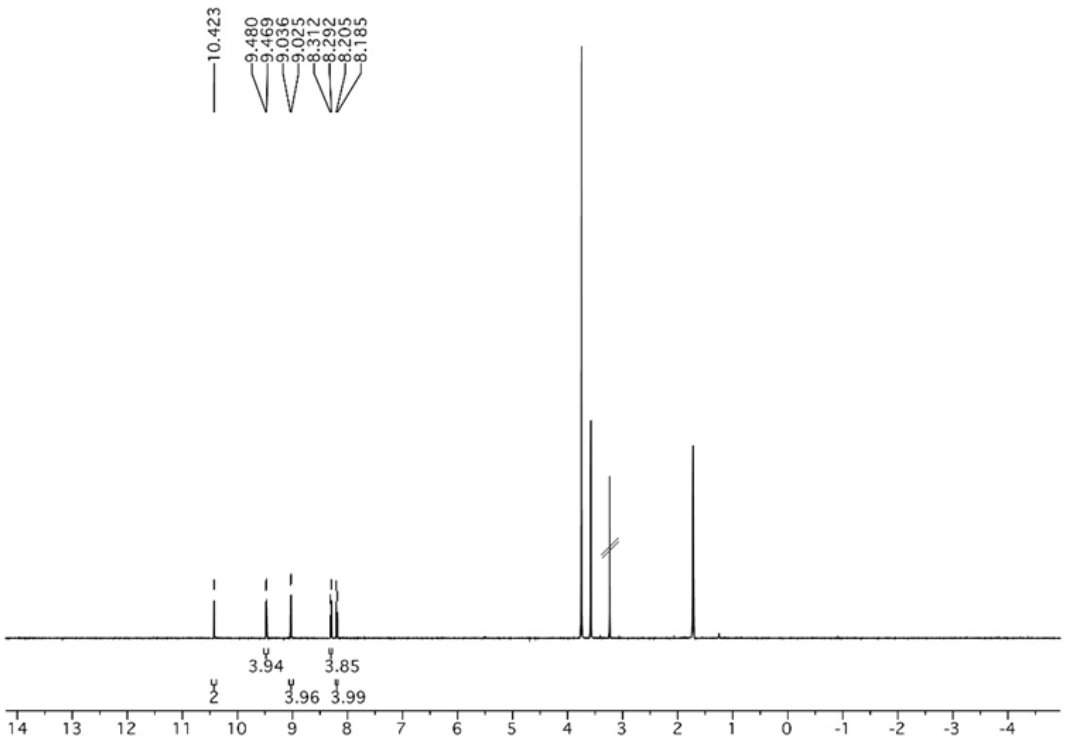

100 MHz, THF-d_8+3 drops of D_2O

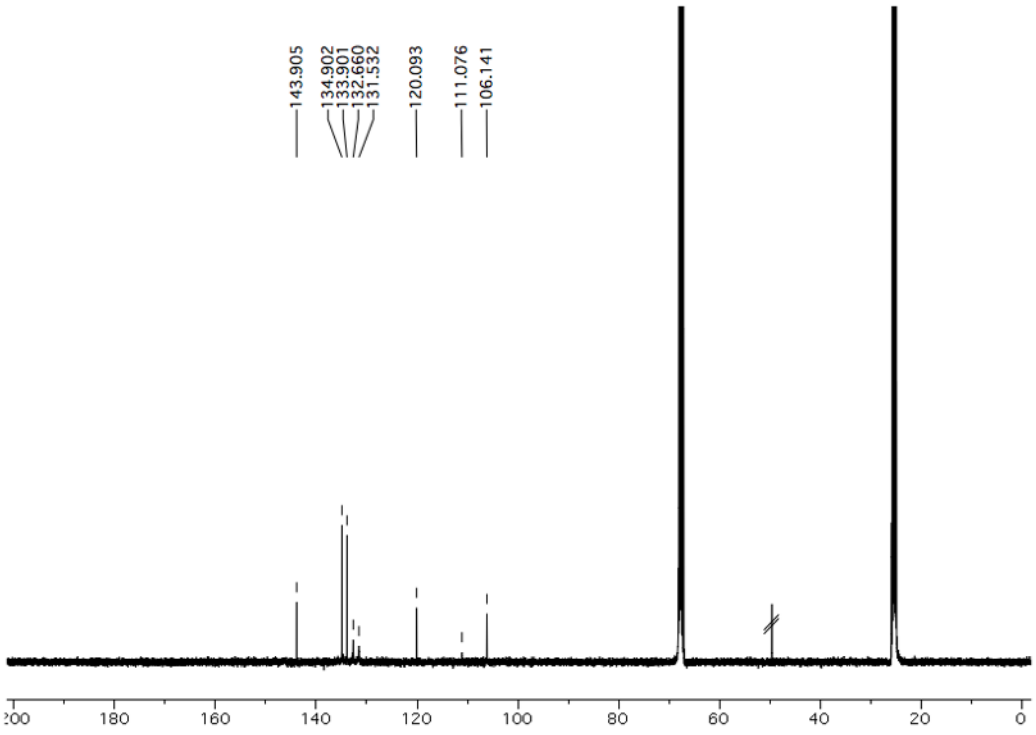

Compound **2**

600 MHz, $CDCl_3$

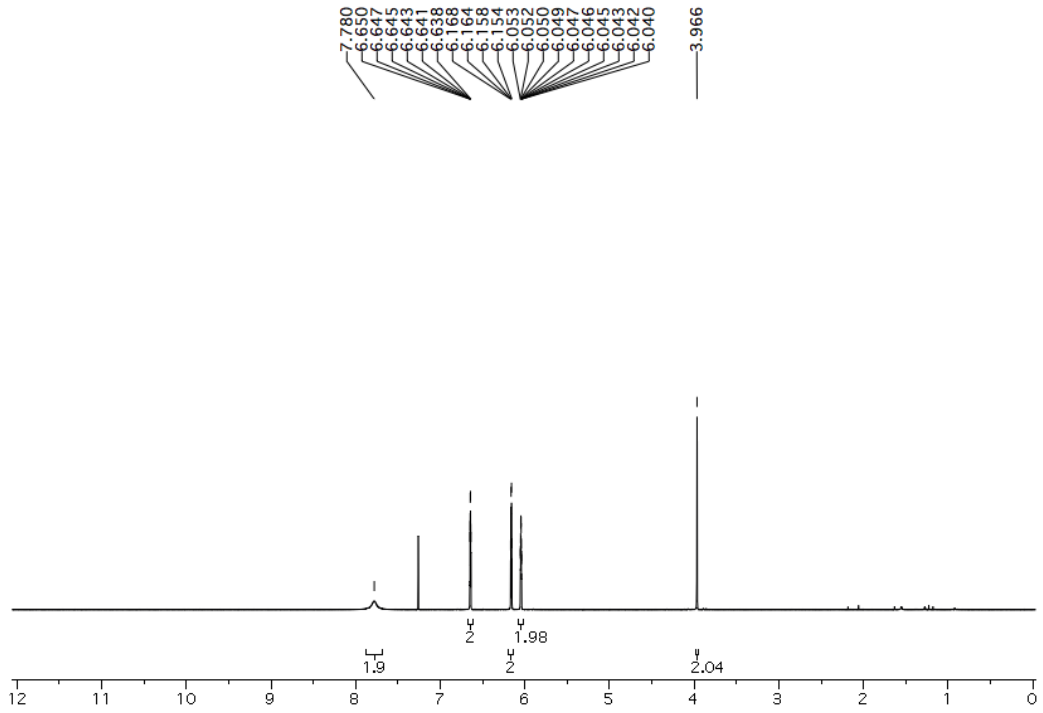

150 MHz, $CDCl_3$

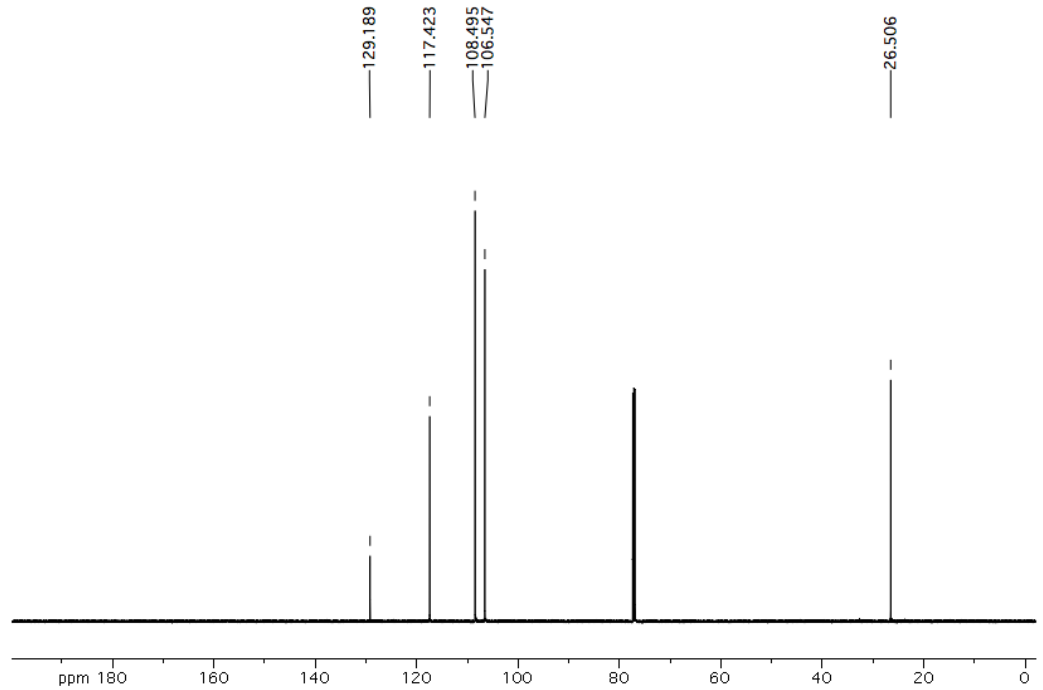

Compound **5**

300 MHz, $CDCl_3$

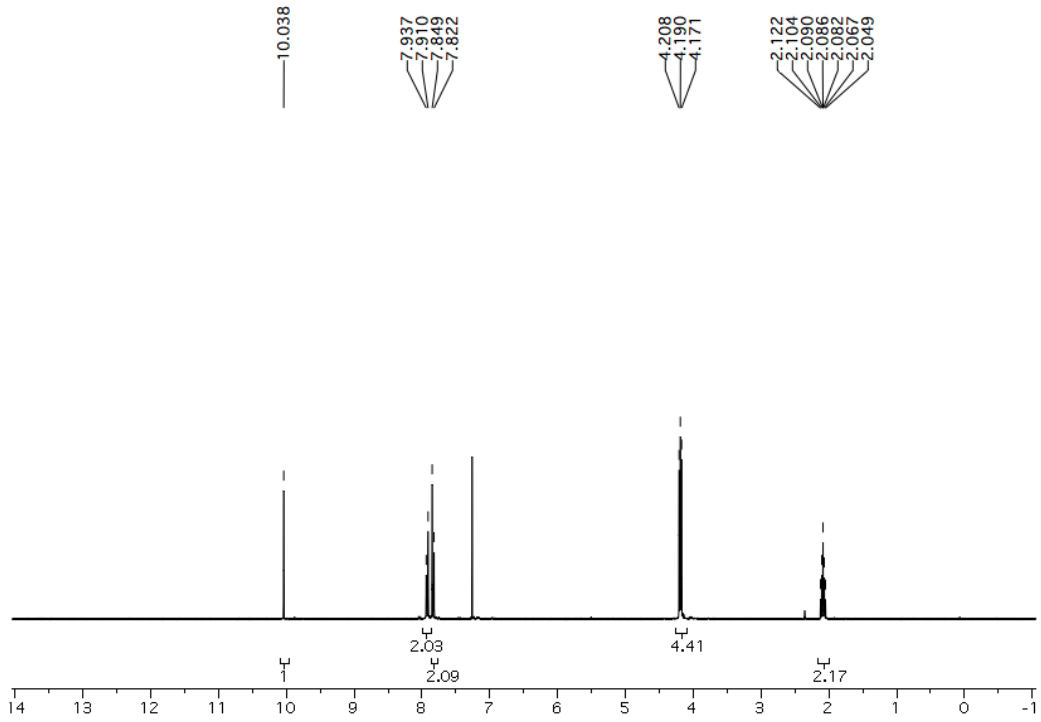

75 MHz, $CDCl_3$

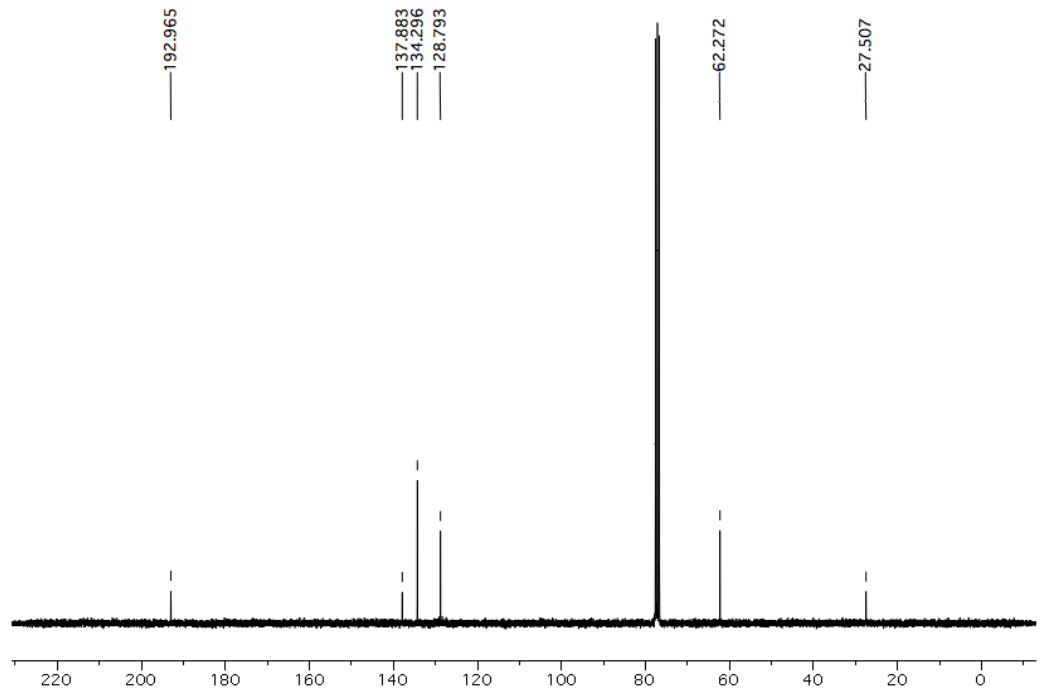

Compound **7**

600 MHz, $CDCl_3$

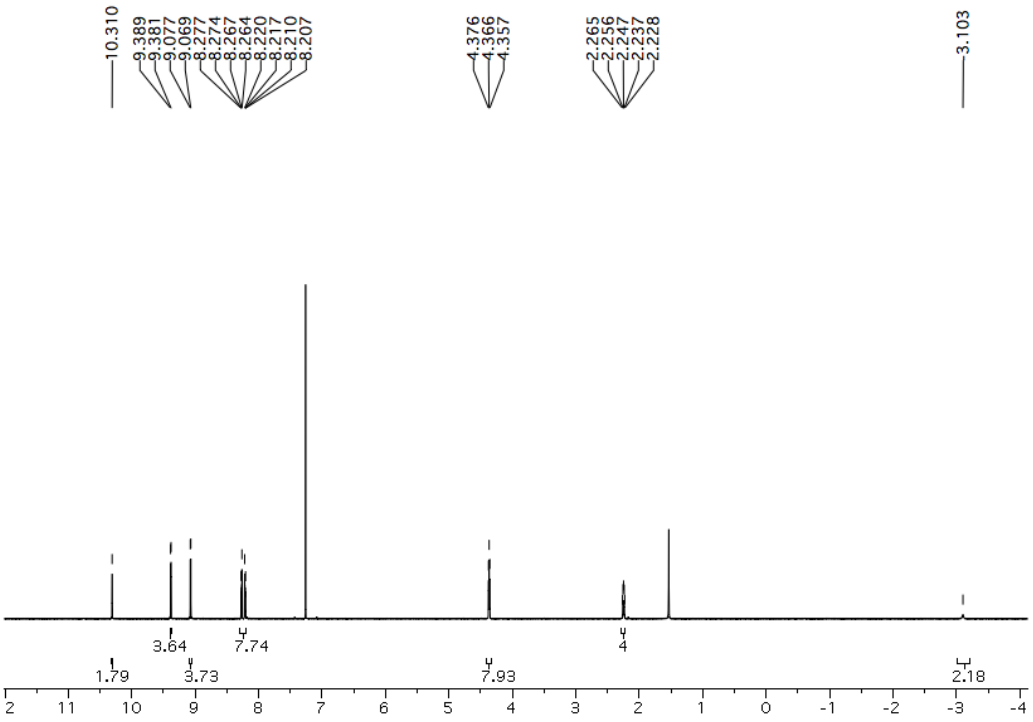

150 MHz, $CDCl_3$

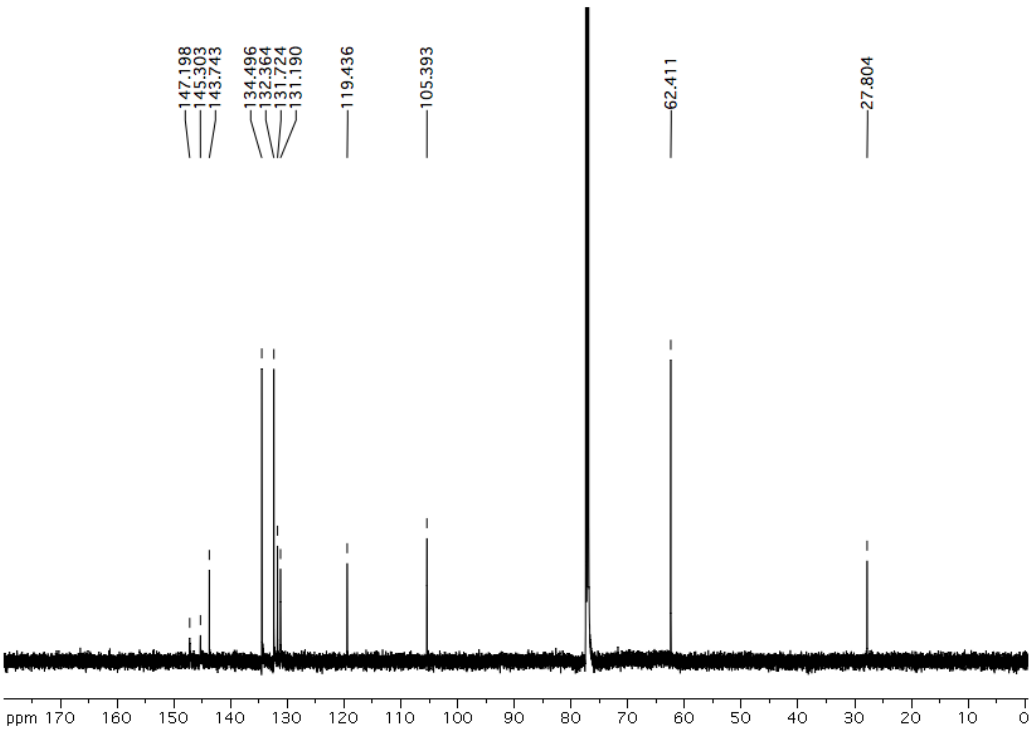

Section 11: References

[1] J. K. Laha, S. Dhanalekshmi, M. Taniguchi, A. Ambroise, J. S. Lindsey, *Org. Process Res. Dev.* **2003**, *7*, 799–812.

[2] X. Feng, L. Chen, Y. Dong, D. Jiang, *Chem. Commun.* **2011**, *47*, 1979–1981.

[3] T. D. James, K. R. S. Sandanayake, R. Iguchi, S. Skinkai, *J. Am. Chem. Soc.* **1995**, *117*, 8982–8987.

[4] D. Liu, T. Kelly, *Nat. Photon.* **2013**, *8*, 133–138.

[5] M. K. Smith, B. H. Northrop, *Chem. Mater.* **2014**, *26*, 3781–3795.